



Short Communication

Observation and quantification of the diffusion-induced grain boundary migration ahead of SCC crack tips

Zhao Shen^{a,*}, Phani Karamched^a, Koji Arioka^b, Sergio Lozano-Perez^a^a Department of Materials, University of Oxford, Parks Road, OX1 3PH, Oxford, UK^b Institute of Nuclear Safety Systems, Inc. (INSS), 64 Sata, Mihama-cho, Mikata-gun, Fuku, Mihama, 919-1205, Japan

ARTICLE INFO

Keywords:

Nickel alloy

Crack tip

Diffusion-induced grain boundary migration

Oxidation

Transmission electron microscopy

ABSTRACT

Crack tips prepared from Ni-based alloys after stress corrosion cracking testing in simulated pressurized water reactor primary water have been studied by high-resolution characterization. Diffusion-induced grain boundary migration (DIGM) was observed in all the cracks and its potential role on the crack propagation is discussed in detail. The extent of DIGM observed changed with grain boundary type and alloy composition, which could lead to different extent of retardation effects on the crack propagation. A method is proposed to quantify the role of DIGM on crack propagation based on the results obtained in this work.

Ni-based alloys have been extensively used in the nuclear industry as structural components due to their combination of excellent mechanical properties and high corrosion resistance [1]. Although these alloys have a good service record, many become susceptible to stress corrosion cracking (SCC) under pressurized water reactor (PWR) primary water conditions. To obtain a mechanistic understanding of the SCC behavior, a large amount of work has been conducted over the last several decades. Among them, water chemistry, materials composition, temperature, cold work, and intergranular carbides were considered to play important roles in SCC [2–11]. Recently, grain boundary migration (GBM) has been reported on Ni-based alloys and stainless steels after exposure to simulated PWR primary water at 300–360 °C [6–9,12]. GBM was also reported in Ni-based alloys after tested in a high temperature hydrogenated steam at 480 °C, designed to simulate PWR primary water conditions, although easier to set up [13–16]. In-situ transmission electron microscopy (TEM) confirmed that the presence of hydrogen in the environment was essential for this phenomenon to occur [17] since they could not reproduce it when exposed to pure N₂. The GBM zone observed in the high temperature aqueous environment was always depleted in Cr and Fe and enriched in Ni, which is very similar to the results reported by Balluffi and Cahn [18] where the process of GBM was driven by the diffusion of solute elements. Due to the similarities between the GBM occurring in the high temperature aqueous environment and Balluffi and Cahn's observations, it has also been referred to as diffusion-induced GBM (DIGM) [7,8,12–17], which will be used from now on in this manuscript.

Although a lot of work has been conducted to understand the

potential roles of DIGM in the SCC, it has mainly focused on how it affects intergranular oxidation rate [8,9,13–16]. However, a higher intergranular oxidation rate might not necessarily lead to a higher SCC crack growth rate (CGR), which is a more important parameter to the mechanistic understanding of SCC and to the industry. To obtain a more direct understanding of the relationship between DIGM and SCC crack propagation, it is essential to make experimental observations of DIGM around the crack tips [12,19–22]. In the current study, high-resolution analytical TEM (ATEM) and transmission Kikuchi diffraction (TKD) were used to study the chemistry and metallography around SCC crack tips. With these direct observations, the potential role of DIGM on the SCC propagation can be better explained.

A 20% cold-worked Alloy 60Ni has been chosen for this study since it exhibits an unusually high level of DIGM at crack tips combined with a lower CGR when compared to similar austenitic alloys under the same testing conditions [3]: simulated PWR primary water conditions (hydrogenated water: 500 ppm B + 2 ppm Li + 30 cc/kg dissolved H₂) at 360 °C. The SCC test was conducted by INSS (Japan) using a pre-cracked 0.5 T compact tension (CT) specimen in the T-L direction (crack growth direction parallel to the rolling direction) in an autoclave under a constant load of 30 MPa m^{1/2}. More details can be found in [3]. The material was solution-treated at 1075 °C for 1 h in air and water-cooled. It has a chemical composition of 0.026 C, 0.28 Si, 0.41 Mn, 0.002 P, 0.001 S, 16.17 Cr, 23.05 Fe, and balance Ni (wt. %). The microstructure of the material is shown in Fig. 1a and b, revealing that the deformation is preferentially distributed along the GBs after prior 20% of cold-work. The average grain size of this material was around 300 μm. After the

* Corresponding author.

E-mail address: zhao.shen@materials.ox.ac.uk (Z. Shen).<https://doi.org/10.1016/j.corsci.2018.11.019>

Received 5 August 2018; Received in revised form 21 November 2018; Accepted 23 November 2018

Available online 26 November 2018

0010-938X/ © 2019 The Authors. Published by Elsevier Ltd. This is an open access article under the CC BY license (<http://creativecommons.org/licenses/by/4.0/>).

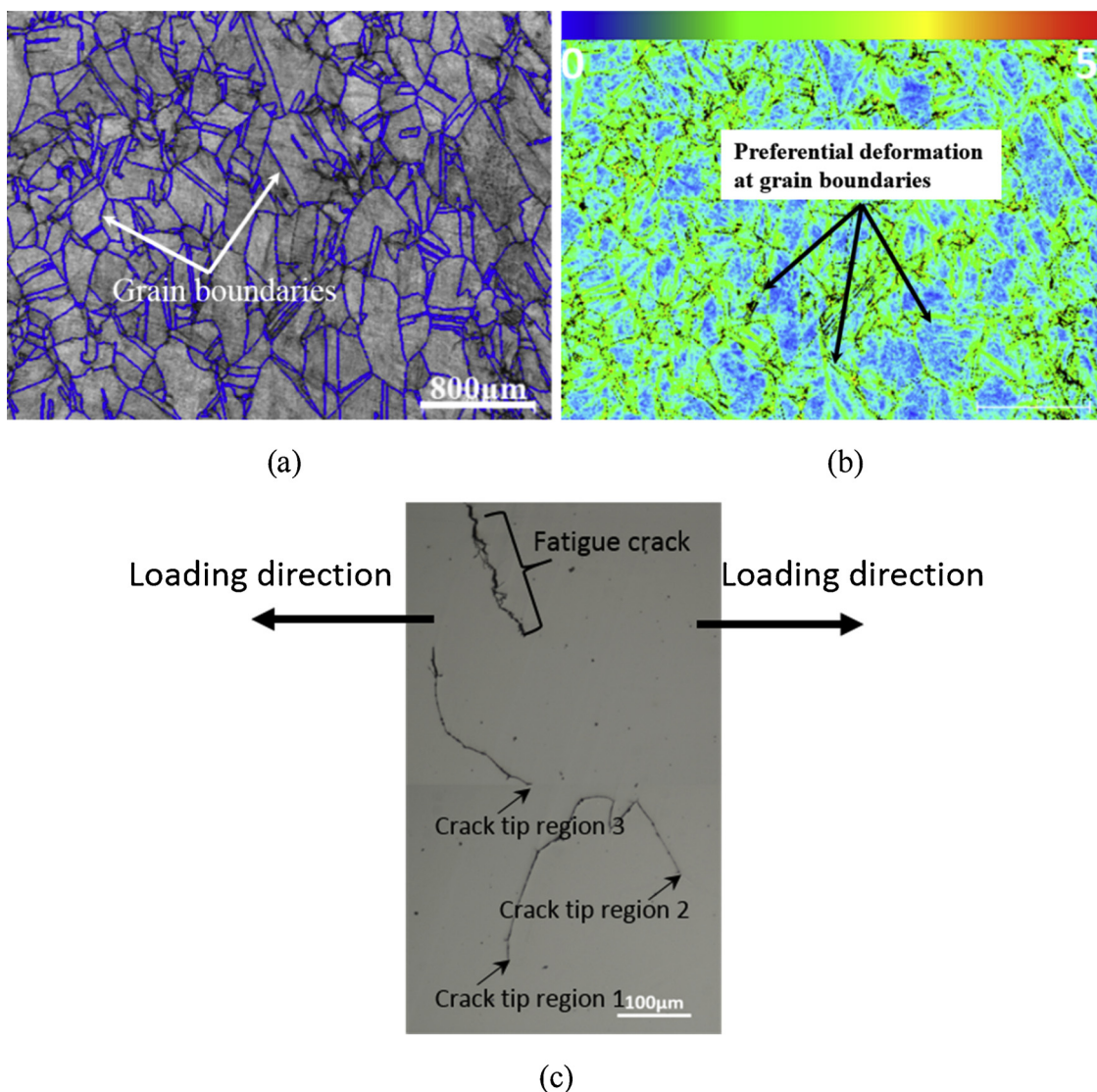


Fig. 1. Microstructure of Alloy 60Ni obtained from EBSD analysis: a) pattern quality map with GBs (blue lines); b) kernel misorientation (KMO) map. c) Optical micrograph of SCC crack cross-section of Alloy 60Ni after SCC testing. (For interpretation of the references to colour in this figure legend, the reader is referred to the web version of this article).

autoclave testing the surface containing the SCC cracks was well-polished to obtain a mirror-finished surface, as shown in Fig. 1b.

Focused ion beam (FIB) was used to prepare TEM foils containing SCC crack tips. More details about the sample preparation technique can be found in [23]. Once crack tip samples were prepared, high-resolution scanning TEM (STEM) and electron energy loss spectroscopy (EELS) were conducted with a JEOL ARM200F (cold-field emission gun) operating at 200 kV and equipped with a Quantum Gatan image filter spectrometer. TKD was performed using a Zeiss Crossbeam 540 FEG-SEM equipped with an Oxford Instrument electron back scattered diffraction (EBSD) NordlysMax 3 detector.

Fig. 1c shows the cross-section of the SCC cracks with the location of crack tips. The SCC crack was not continuous in 2 dimensional (2D) and crack branching was observed. Further observation reveals that the crack tip region 1 was deeper than the crack tip region 2, indicating that the CGRs along these two branches were different. To understand this difference in CGRs in the two branches, high-resolution characterization was essential. In this study, crack tips are defined as the last portion of the GB (oxidized or not) directly exposed to the environment. To identify the position of crack tips in the TEM samples, STEM dark-field imaging combined with Fresnel contrast in TEM mode were used [20].

Fig. 2a shows the crack tip prepared from region 1 (see Fig. 1c). The HAADF image shows that the crack had a tortuous shape. The EELS Ni-map shows that the curved shape of the crack was the result of DIGM. Once DIGM occurred, the crack started to propagate along the migrated GB. Bertali et al. [13–16] and Langelier et al. [17] also observed DIGM at the oxidized GB of Alloy 600 after exposed to the high-temperature hydrogenated steam, although SCC cracks were not observed in these studies. Along the crack flanks in Fig. 2a, penetrative oxidation was observed (towards the matrix) and the maximum penetrative oxidation depth was around 300 nm. Similar phenomenon was also observed by Kuang et al. [12] on the surface of Alloy 690 and by Bertali et al. [14] on the surface of Alloy 600. The authors attributed the penetrative oxidation to the low protectiveness of the surface oxide. Further observation around the crack tip region (region 1 in Fig. 2a) with higher resolution exhibits that the penetrative oxidation on the crack flanks stopped at a specific point, coinciding with the crack tip. The original and migrated GBs were highlighted by blue and red dashed lines, respectively (see Fig. 2b). Ahead of the crack tip, an intergranular oxidation zone (IOZ) along the migrated GB with a length of around 300 nm was observed, which was also reported in the literature [12,19,20,24,25]. The reason for no penetrative oxidation ahead of the

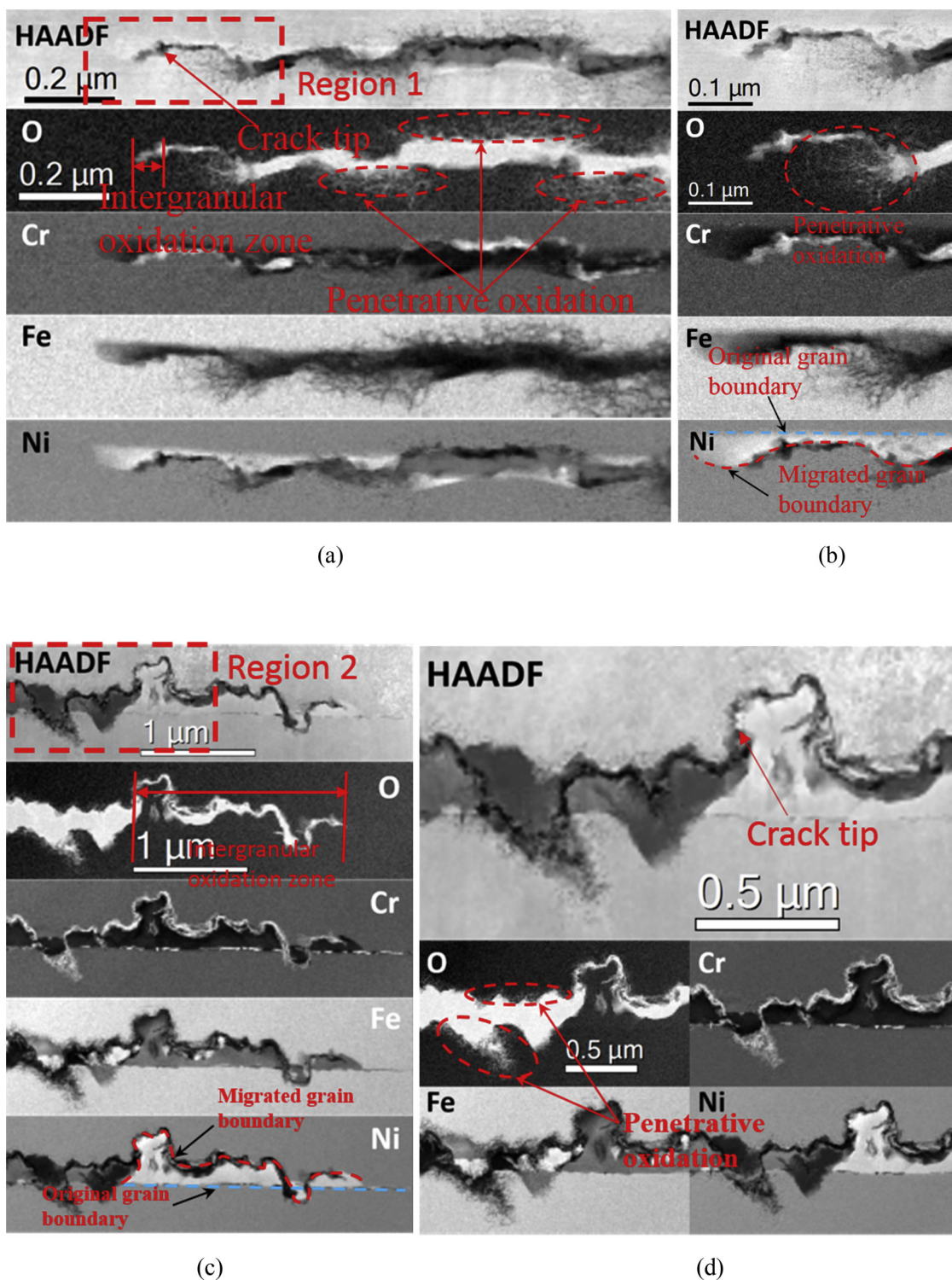


Fig. 2. a) HAADF and EELS elemental images of crack tip 1; b) HAADF and EELS elemental images of region 1 in a); c) HAADF and EELS elemental images of crack tip 2; d) HAADF and EELS elemental images of region 2 in c).

crack tip might be due to the low oxidation potential in this part of region or not enough time in contact with the environment. Compared with the penetrative oxidation, oxidation along the GB appears to have occurred faster (due to a higher defect density). However, once a crack occurred, the crack flanks were directly exposed to the high-temperature water, which then enabled the observed penetrative oxidation to happen. This hypothesis could be supported by the results reported in literature that penetrative oxidation was only observed under the

surface that was directly exposed to the water but not observed in the region close to the oxidized GB without cracking [13–16].

Fig. 3a shows a crack tip prepared from region 2 (see Fig. 1b). DIGM at this GB seemed to be more intensive than that observed in region 1 (Fig. 2a). Penetrative oxidation in the crack flanks was also observed and stopped at a specific point. This point was identified as the crack tip of this crack (see Fig. 3b). An IOZ with a length of around 1.8 μm was observed ahead of the crack tip, which was much longer than what was

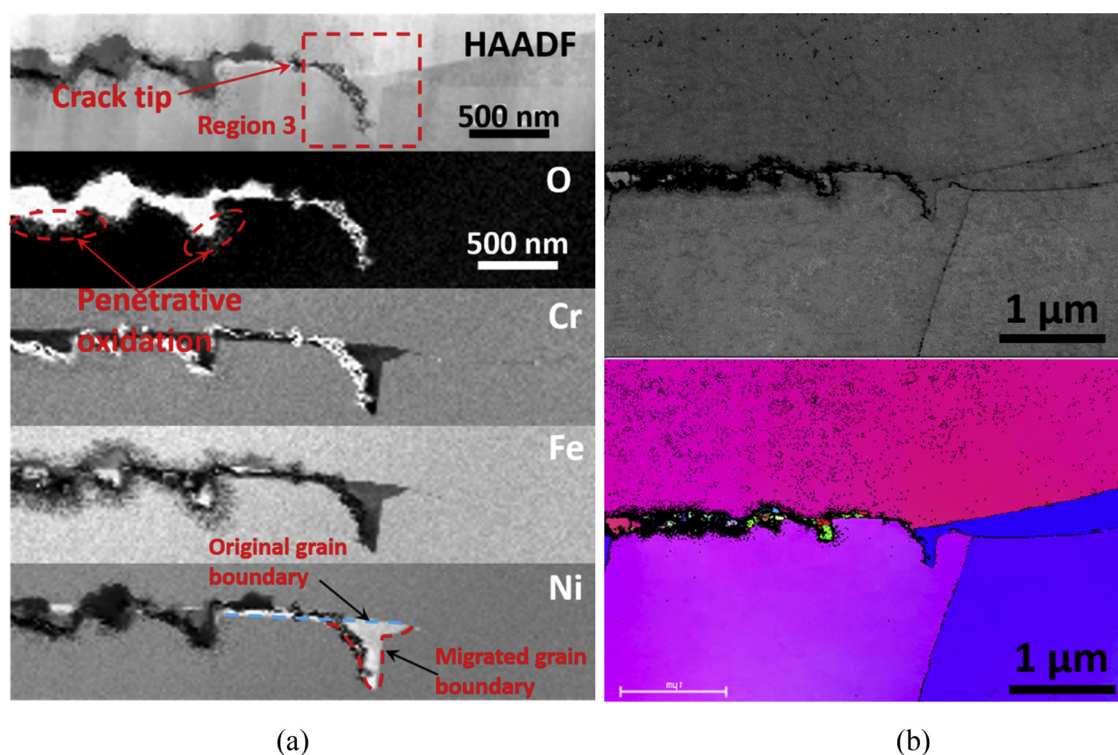


Fig. 3. a) HAADF and elemental images of crack tip 3; b) TKD maps containing the crack tip 3 (Top: pattern quality map; Bottom: IPFZ map).

observed in Fig. 2b. Further observation reveals that the crack propagation was not along the original GB but the migrated GB because the intergranular oxidation occurred along the migrated GB instead of the original GB. This is consistent to what was reported by Bertali et al. [13–15] and Kuang et al. [12]. In addition, the authors considered that the DIGM could enhance the intergranular oxidation, which then increased the SCC susceptibility. According to this conclusion, the crack tip 2 should exhibit higher SCC susceptibility than the crack tip 1 since the DIGM at the crack path 2 seemed to be more intensive than the crack path 1. However, from our current observations of crack propagation, crack 1 advanced further than crack 2, which contradicts the above theory meaning there should be additional factors contributing to the lower CGR along the crack path 2.

Although cracks 1 and 2 are the ones that propagated deeper into the sample, the exposure time for the two crack tips might be different due to their different CGRs. However, according to Langelier et al. [16], the extent of DIGM is mainly affected by the characteristics of the GB itself but not the exposure time. Similar results were also observed in the current study. As shown in the supplementary data, the DIGM of an inactive crack tip (longer exposure time) was not more intensive than that in the crack tips 1 and 2 (see Figs. 2 and S1). Consequently, the effect of the different exposure time on the two crack tips might be negligible. According to the result reported by Stratulat et al. [26], the SCC susceptibility of a specific GB can be affected by the GB orientation relative to the applied stress direction. The two GBs studied here in the Fig. 1b exhibited similar orientation relative to the applied stress direction. As a result, its potential effect on the SCC susceptibility should be similar. In addition, the GB character type was also reported to affect the SCC susceptibility [27]. However, the TKD analysis on these two crack tip samples revealed that the two GBs were high angle GBs. As a result, the effect of the GB character type is not enough to explain the differences in propagation.

In studies involving the effect of intergranular carbides on SCC, Was et al. [28] and Dugdale et al. [29] suggested that the existence of intergranular carbides created a more tortuous path for the intergranular crack propagation, which could reduce the CGR by locally reducing the

effective applied stress and physically hindering the crack propagation. Compared to the intergranular carbides, the DIGM could play a similar role because it forces the crack to follow a “wavy” migrated GB, as opposed to the original “straight” one. Although the higher extent of DIGM could accelerate the intergranular oxidation, a more tortuous migrated GB could not only physically hinder the crack propagation but also increase the total crack path, which could finally lead to a lower CGR.

To further confirm our hypothesis that the DIGM could lead to the retardation of SCC propagation, a TEM sample was prepared from a potential inactive crack tip at region 3 (see Fig. 1b). The HAADF image reveals that the crack propagation diverged from the original GB plane (see Fig. 3a). The EELS maps show that the divergence of crack propagation was the result of DIGM. As shown in the Ni-map (see Fig. 3a), the sudden DIGM protrusion diverged the crack propagation from the original crack path to a very sharp corner, which could have led to its arrest. TKD analysis around the crack tip region is shown in the Fig. 3b. Comparing the DIGM in the regions 1 and 2 to that in region 3, the latter seemed to be more intense. The inverse pole figure (z-axis) (IPFZ) map in the Fig. 3b revealed that accelerated DIGM occurred in the region 3 might be because it is located close to a GB triple point. According to the results reported in literature [6,8,12–16], the DIGM is the result of elemental diffusion. At a triple point, diffusion of solute elements (Cr and Fe) was more available, resulting in the formation of a more intense DIGM, as shown in Fig. 3.

A Ni-rich zone was also reported in 304 stainless steel after exposed to PWR primary water and the oxidation along the original GB was observed to be effectively mitigated by the Ni-rich zone [9]. As a result, the authors proposed that the formation of Ni-rich zone at the front of the oxidized GBs could reduce the intergranular oxidation rate and then decrease the SCC CGR, which contradict to the results observed in this study and in the literature [6,8,12–16]. This discrepancy might come from the lack of examination of the newly formed migrated GBs in [9], since the oxidation of the original GBs was also terminated in the current study and in the literature [6,8,12–16], while the oxidation along the migrated GBs was remarkably enhanced.

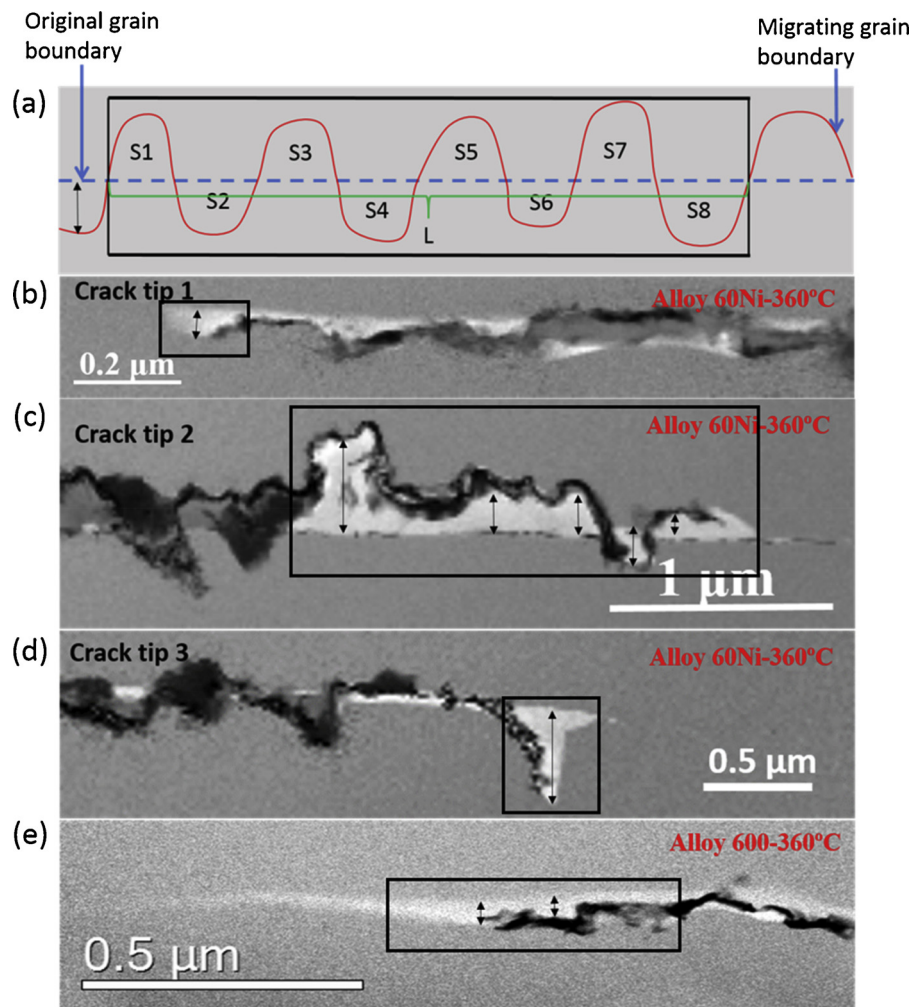


Fig. 4. a) Schematic illustration of DIGM with many protrusions; EELS Ni maps of b) crack tip 1; c) crack tip 2; d) crack tip 3; e) crack tip prepared from Alloy 600.

According to the discussion above, although the DIGM could enhance oxidation along the migrated GBs, the tortuous morphology of the migrated GB could hinder the crack propagation and increase the total crack path, which would decrease the CGR. This “qualitative” observation could be quantified by characterizing the DIGM occurring ahead of the crack tip since, once GB fracture has occurred, crack flank oxidation would mask it. DIGM occurred at a specific GB is schematically shown in Fig. 4a. To quantify the extent of DIGM, an equation is introduced below:

$$D_{\text{DIGM}} = (S1 + S2 + S3 + S4 + S5 + S6 + S7 + S8)/L \quad (1)$$

where D_{DIGM} is DIGM induced deviation from the original GB; S_n ($n = 1, 2, 3, 4, 5, 6, 7, 8$) is the area of protrusions induced by DIGM; L is the length of the original GB. EELS Ni maps of the crack tips 1, 2, and 3 are presented in Fig. 4b–d, respectively. According to the Eq. (1), the calculated D_{DIGM} ahead of crack tips 1, 2, and 3 were 45.8 nm, 164.7 nm, and 213.2 nm, respectively. This (anti) correlates well with the degree of propagation these cracks exhibited. The higher the extent of DIGM (particularly in the direction perpendicular to the grain boundary plane), the more the cracks were slowed down. DIGM was also observed in Alloy 600 exposed to the similar PWR primary water condition reported in a previous work [12] (see Fig. 4e) and the calculated D_{DIGM} was 31.1 nm, much lower than in the Alloy 60Ni in this work. It is therefore suggested that the retardation introduced by DIGM is only effected after a minimum D_{DIGM} is achieved ahead of the crack tip, which did not happen for Alloy 600, exhibiting a much higher CGR than Alloy 60Ni.

In summary, DIGM was observed in all the examined GBs. After the DIGM, the migrated GB is oxidized and crack propagation is observed to develop along the migrated GB, which is no longer straight and often “tortuous”. The DIGM can be affected by a lot of factors, resulting in different extent of DIGM at different GBs, even in the same material. Although DIGM could accelerate the intergranular oxidation, the formation of tortuous migrated GB changes the crack propagation direction and the effective stress it experiences ultimately decreasing the CGR. With the method proposed in this work, it is possible to quantify the role of DIGM on CGR of different materials, which would be very helpful in building an empirical model to predict the service time of a specific structural materials used in the PWR primary water conditions.

Acknowledgements

The authors would like to thank INSS (Japan) for providing the sample used in this study and for useful discussions. Zhao Shen is also grateful to China Scholarship Council, China; EPSRC, UK for providing financial support. The EPSRC (EP/K040375/1, EP/N010868/1 and EP/R009392/1) grants are also acknowledged for funding this research.

References

- [1] V.Y. Gertsman, S.M. Brummer, Study of grain boundary character along intergranular stress corrosion crack paths in austenitic alloys, *Acta Mater.* 49 (2001) 1589–1598.
- [2] P.L. Andresen, M.M. Morra, Stress corrosion cracking of stainless steels and nickel alloys in high-temperature water, *Corrosion*. 64 (2008) 15–29.

- [3] K. Arioka, T. Yamada, T. Miyamoto, M. Aoki, Intergranular stress corrosion cracking growth behavior of Ni-Cr-Fe alloys in pressurized water reactor primary water, *Corrosion*. 70 (2014) 695–707.
- [4] S. Lozano-Perez, K. Kruska, I. Iyengar, T. Terachi, T. Yamada, The role of cold work and applied stress on surface oxidation of 304 stainless steel, *Corros. Sci.* 56 (2012) 78–85.
- [5] T. Terachi, T. Yamada, T. Miyamoto, K. Arioka, SCC growth behaviors of austenitic stainless steels in simulated PWR primary water, *J. Nucl. Mater.* 426 (2012) 59–70.
- [6] M.J. Olszta, D.K. Schreiber, L.E. Thomas, S.M. Bruemmer, Springer, Cham Proceedings of the 15th International Conference on Environmental Degradation of Materials in Nuclear Power Systems—Water Reactors 2011, Proceedings of the 15th International Conference on Environmental Degradation of Materials in Nuclear Power Systems—Water Reactors (2011) 1503–1517.
- [7] D.K. Schreiber, M.J. Olszta, S.M. Bruemmer, Directly correlated transmission electron microscopy and atom probe tomography of grain boundary oxidation in a Ni–Al binary alloy exposed to high-temperature water, *Scripta Mater.* 69 (2013) 509–512.
- [8] S.Y. Persaud, J. Smith, A. Korinek, G.A. Botton, R.C. Newman, High resolution analysis of oxidation in Ni-Fe-Cr alloys after exposure to 315° C deaerated water with added hydrogen, *Corros. Sci.* 106 (2016) 236–248.
- [9] K. Kruska, S. Lozano-Perez, D.W. Saxey, T. Terachi, T. Yamada, G.D.W. Smith, Nanoscale characterisation of grain boundary oxidation in cold-worked stainless steels, *Corros. Sci.* 63 (2012) 225–233.
- [10] L. Fournier, O. Calonne, P. Combrade, P. Scott, P. Chou, R. Pathania, Springer, Cham Proceedings of the 15th International Conference on Environmental Degradation of Materials in Nuclear Power Systems—Water Reactors 2011, Proceedings of the 15th International Conference on Environmental Degradation of Materials in Nuclear Power Systems—Water Reactors (2011).
- [11] S. Attanasio, D. Morton, Stevenson (Washington) Proceedings of the 11th International Conference on Environmental Degradation of Materials in Nuclear Power Systems—Water Reactors 2003, Proceedings of the 11th International Conference on Environmental Degradation of Materials in Nuclear Power Systems—Water Reactors (2003).
- [12] W. Kuang, M. Song, G.S. Was, Insights into the stress corrosion cracking of solution annealed alloy 690 in simulated pressurized water reactor primary water under dynamic straining, *Acta Mater.* 151 (2018) 321–333.
- [13] G. Bertali, F. Scenini, M.G. Burke, The intergranular oxidation susceptibility of thermally-treated Alloy 600, *Corros. Sci.* 114 (2017) 112–122.
- [14] G. Bertali, F. Scenini, M.G. Burke, The effect of residual stress on the preferential intergranular oxidation of alloy 600, *Corros. Sci.* 111 (2016) 494–507.
- [15] G. Bertali, F. Scenini, M.G. Burke, Advanced microstructural characterization of the intergranular oxidation of Alloy 600, *Corros. Sci.* 100 (2015) 474–483.
- [16] B. Langelier, S.Y. Persaud, A. Korinek, T. Casagrande, R.C. Newman, G.A. Botton, Effects of boundary migration and pinning particles on intergranular oxidation revealed by 2D and 3D analytical electron microscopy, *Acta Mater.* 131 (2017) 280–295.
- [17] M.G. Burke, G. Bertali, E. Prestat, F. Scenini, S.J. Haigh, The application of in situ analytical transmission electron microscopy to the study of preferential intergranular oxidation in alloy 600, *Ultramicroscopy* 176 (2017) 46–51.
- [18] R.W. Balluffi, J.W. Cahn, Mechanism for diffusion induced grain boundary migration, *Acta Metal.* 29 (1981) 493.
- [19] M. Sennour, P. Laghoutaris, C. Guerre, R. Molins, Advanced TEM characterization of stress corrosion cracking of Alloy 600 in pressurized water reactor primary water environment, *J. Nucl. Mater.* 393 (2009) 254–266.
- [20] Z. Shen, K. Arioka, S. Lozano-Perez, A mechanistic study of SCC in Alloy 600 through high-resolution characterization, *Corros. Sci.* 132 (2018) 244.
- [21] M. Meisnar, A. Vilalta-Clemente, M. Moody, K. Arioka, S. Lozano-Perez, A mechanistic study of the temperature dependence of the stress corrosion crack growth rate in SUS316 stainless steels exposed to PWR primary water, *Acta Mater.* 114 (2016) 15–24.
- [22] S. Lozano-Perez, T. Yamada, T. Terachi, M. Schröder, C.A. English, G.D.W. Smith, C.R.M. Grovenor, B.L. Eyre, Multi-scale characterization of stress corrosion cracking of cold-worked stainless steels and the influence of Cr content, *Acta Mater.* 57 (2009) 5361–5381.
- [23] S. Lozano-Perez, A guide on FIB preparation of samples containing stress corrosion crack tips for TEM and atom-probe analysis, *Micron* 39 (2008) 320–328.
- [24] L.E. Thomas, S.M. Bruemmer, High-resolution characterization of intergranular attack and stress corrosion cracking of Alloy 600 in high-temperature primary water, *Corrosion* 56 (2000) 572–587.
- [25] S.M. Bruemmer, E.P. Simonen, P.M. Scott, P.L. Andresen, G.S. Was, J.L. Nelson, Radiation-induced material changes and susceptibility to intergranular failure of light-water-reactor core internals, *J. Nucl. Mater.* 274 (1999) 299–314.
- [26] A. Stratulat, J.A. Duff, T.J. Marrow, Grain boundary structure and intergranular stress corrosion crack initiation in high temperature water of a thermally sensitised austenitic stainless steel, observed in situ, *Corros. Sci.* 8 (2014) 428–435.
- [27] V.Y. Gertsman, S.M. Bruemmer, Study of grain boundary character along intergranular stress corrosion crack paths in austenitic alloys, *Acta Mater.* 49 (2001) 1589–1598.
- [28] G.S. Was, K. Lian, Role of carbides in stress corrosion cracking resistance of Alloy 600 and controlled-purity Ni-16% Cr-9% Fe in primary water at 360° C, *Corrosion* 54 (1998) 675–688.
- [29] H. Dugdale, D.E. Armstrong, E. Tarleton, S.G. Roberts, S. Lozano-Perez, How oxidized grain boundaries fail, *Acta Mater.* 61 (2013) 4707–4713.